

## Supporting Information

# The Competition Between Mechanical Stability and Charge Carrier Mobility in MA-based Hybrid Perovskites: Insight from DFT

Jung-Hoon Lee,<sup>\*‡<sup>a</sup></sup> Zeyu Deng,<sup>‡<sup>a</sup></sup> Nicholas C. Bristowe,<sup>b,c</sup>  
Paul D. Bristowe,<sup>\*<sup>a</sup></sup> and Anthony K. Cheetham<sup>\*<sup>a</sup></sup>

<sup>a</sup>*Department of Materials Science and Metallurgy, University of Cambridge,  
Cambridge CB3 0FS, UK*

<sup>b</sup>*School of Physical Sciences, University of Kent, Canterbury  
CT2 7NH, UK*

<sup>c</sup>*Department of Materials, Imperial College London, London SW7 2AZ, UK*

\*E-mail: [jhlee.david@gmail.com](mailto:jhlee.david@gmail.com), [pdb1000@cam.ac.uk](mailto:pdb1000@cam.ac.uk), [akc30@cam.ac.uk](mailto:akc30@cam.ac.uk).

‡These authors contributed equally.

## 1. van der Waals functionals

**Table S1** | Computed lattice parameters and the polycrystalline (orientationally-averaged) Young's moduli  $E$  of the orthorhombic (*o*-)MAPbI<sub>3</sub> structure using different exchange-correlation functionals compared to experiment.

Functionals	Lattice parameters			$E$ (GPa)
	$a$ (Å)	$b$ (Å)	$c$ (Å)	
PBEsol <sup>1</sup>	8.9762	12.6134	8.4362	20.087
optB86b+vdW <sup>2,3</sup>	8.8576	12.6751	8.5610	20.526
vdW-DF2 <sup>4</sup>	9.2098	13.1736	8.8246	18.201
TS <sup>5</sup>	8.9843	12.7192	8.4960	22.677
SCAN <sup>6</sup>	8.9474	12.7222	8.6123	
Exp. <sup>7</sup>	8.8657	12.6293	8.5769	-

## 2. Ionic radii

**Table S2** | A comparison of computed effective radii of all ions obtained from our DFT calculations with those obtained from Shannon's work.<sup>8</sup>

A-site	Radius (Å)		B-site	Radius (Å)		X-site	Radius (Å)	
	This work	Shannon's radii		This work	Shannon's radii		This work	Shannon's radii
K <sup>+</sup>	1.31	1.55	Sn <sup>2+</sup>	1.39	-	Cl <sup>-</sup>	2.04	1.78
Rb <sup>+</sup>	1.51	1.63	Pb <sup>2+</sup>	1.41	1.19	Br <sup>-</sup>	2.22	1.96
Cs <sup>+</sup>	1.76	1.78				I <sup>-</sup>	2.47	2.20
Fr <sup>+</sup>	1.87	1.80						
MA <sup>+</sup>	2.07							

### 3. Hydrogen bonding-induced octahedral tilting

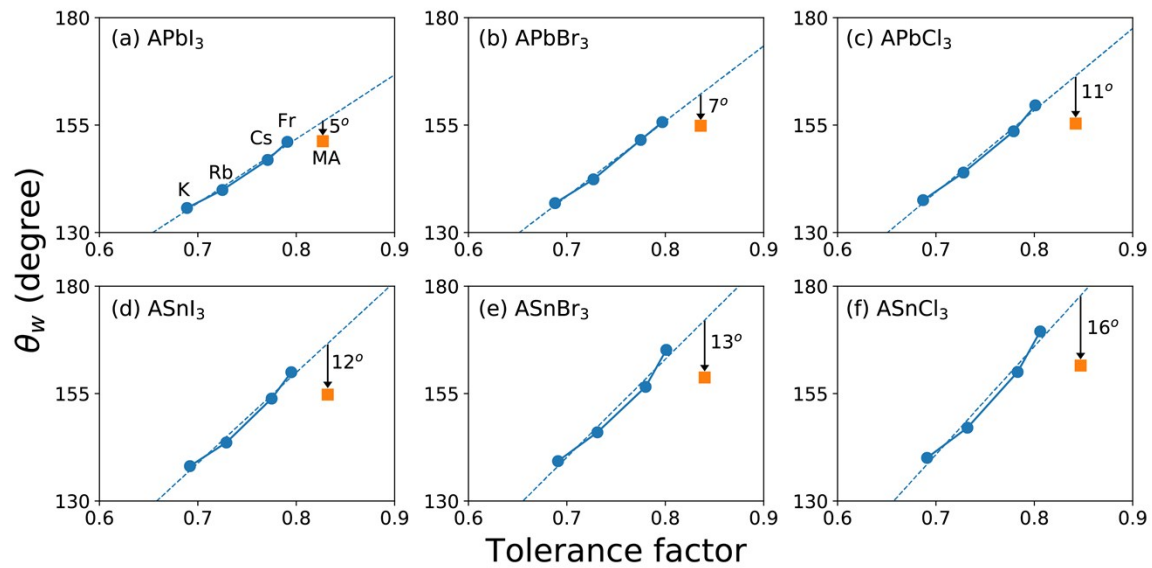


**Figure S1** | Computed average bond angles ( $\theta_w$ ) as a function of the tolerance factor for (a) o-APbI<sub>3</sub>, (b) o-APbBr<sub>3</sub>, (c) o-APbCl<sub>3</sub>, (d) o-ASnI<sub>3</sub>, (e) o-ASnBr<sub>3</sub>, and (f) o-ASnCl<sub>3</sub>. Blue circles and orange squares show the inorganic and hybrid series respectively. Variations from the inorganic trend lines are denoted by black arrows with their magnitudes.

#### 4. Enhancement of hydrogen bonding across the halogen series

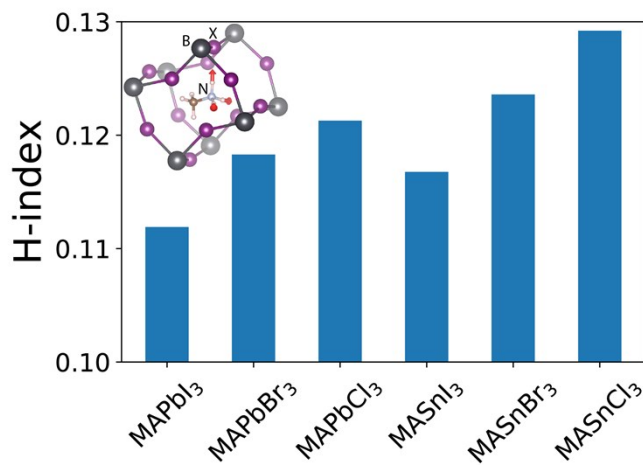


**Figure S2** | Computed average hydrogen-bonding index (H-index) for the three H atoms attached to N on a MA cation for the o-MABX<sub>3</sub> hybrid series. Inset represents a schematic view of the three H stretching modes.

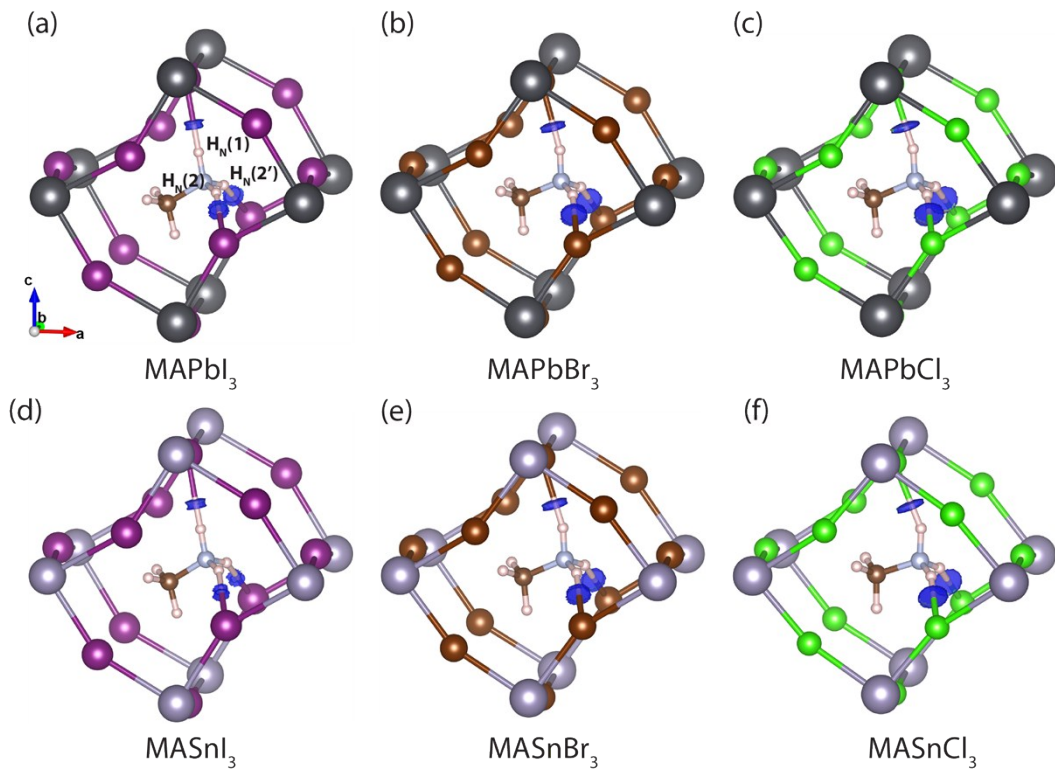


**Figure S3** | Non-covalent interaction density isosurfaces for (a) o-MAPbI<sub>3</sub>, (b) o-MAPbBr<sub>3</sub>, (c) o-MAPbCl<sub>3</sub>, (d) o-MASnI<sub>3</sub>, (e) o-MASnBr<sub>3</sub>, and (f) o-MASnCl<sub>3</sub>. The isosurfaces were generated for  $s = 0.5$  and  $-0.04 < \rho < -0.02$  ( $\rho$  is the electron density and  $s$  is the reduced density gradient).

## 5. 3x3 matrix forms of the six different strain types

$$\begin{aligned}\varepsilon_1 &= \begin{bmatrix} 1+\delta & 0 & 0 \\ 0 & 1 & 0 \\ 0 & 0 & 1 \end{bmatrix}, & \varepsilon_2 &= \begin{bmatrix} 1 & 0 & 0 \\ 0 & 1+\delta & 0 \\ 0 & 0 & 1 \end{bmatrix}, & \varepsilon_3 &= \begin{bmatrix} 1 & 0 & 0 \\ 0 & 1 & 0 \\ 0 & 0 & 1+\delta \end{bmatrix} \\ \varepsilon_4 &= \begin{bmatrix} 1 & 0 & 0 \\ 0 & 1 & \delta/2 \\ 0 & \delta/2 & 1 \end{bmatrix}, & \varepsilon_5 &= \begin{bmatrix} 1 & 0 & \delta/2 \\ 0 & 1 & 0 \\ \delta/2 & 0 & 1 \end{bmatrix}, & \varepsilon_6 &= \begin{bmatrix} 1 & \delta/2 & 0 \\ \delta/2 & 1 & 0 \\ 0 & 0 & 1 \end{bmatrix}\end{aligned}$$

## 6. Directional dependence of the Young's modulus $E$ of o-MAPbI<sub>3</sub> and o-CsPbI<sub>3</sub>

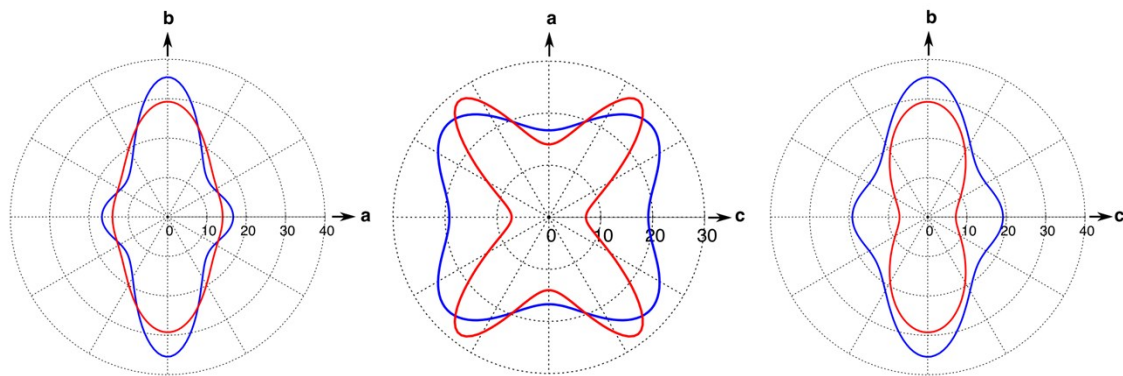


**Figure S4 |** Directionally-dependent Young's modulus  $E$  of o-MAPbI<sub>3</sub> (blue) and o-CsPbI<sub>3</sub> (red) in the *ba*-, *ac*-, and *bc*-planes of the orthorhombic structure. Circles indicate the magnitude of  $E$  (GPa).

## 7. Polycrystalline elastic moduli

**Table S3** | Computed lattice parameters, tolerance factor (TF), the polycrystalline Young's modulus  $E$ , bulk modulus  $B$ , shear modulus  $G$ , and Poisson's ratio  $\nu$  of all halide perovskites. The  $Pnma$  space group was imposed during optimization of the lattice parameters.

	$a$ (Å)	$b$ (Å)	$c$ (Å)	TF	$E$ (GPa)	$B$ (GPa)	$G$ (GPa)	$\nu$
KPbl <sub>3</sub>	8.961	11.887	7.911	0.69	18.455	15.699	7.076	0.304
RbPbl <sub>3</sub>	9.074	12.116	8.001	0.73	16.964	15.107	6.461	0.313
CsPbl <sub>3</sub>	9.142	12.489	8.119	0.77	18.427	15.977	7.045	0.308
FrPbl <sub>3</sub>	9.092	12.608	8.302	0.79	17.342	16.109	6.566	0.321
MAPbl <sub>3</sub>	8.858	12.675	8.561	0.83	20.526	18.999	7.775	0.317
KPbBr <sub>3</sub>	8.379	11.139	7.552	0.69	19.818	18.143	7.519	0.318
RbPbBr <sub>3</sub>	8.481	11.449	7.622	0.73	19.621	17.980	7.443	0.318
CsPbBr <sub>3</sub>	8.483	11.770	7.872	0.78	20.658	19.894	7.784	0.327
FrPbBr <sub>3</sub>	8.450	11.882	8.000	0.80	20.028	20.669	7.482	0.339
MAPbBr <sub>3</sub>	8.543	11.959	7.971	0.84	24.798	22.853	9.399	0.319
KPbCl <sub>3</sub>	7.986	10.674	7.234	0.69	21.977	21.144	8.282	0.327
RbPbCl <sub>3</sub>	8.078	10.943	7.387	0.73	21.296	21.592	7.972	0.336
CsPbCl <sub>3</sub>	8.077	11.282	7.613	0.78	21.876	23.184	8.146	0.343
FrPbCl <sub>3</sub>	7.975	11.346	7.849	0.80	22.807	24.609	8.475	0.346
MAPbCl <sub>3</sub>	8.252	11.442	7.588	0.84	26.119	25.575	9.821	0.330
KSnI <sub>3</sub>	8.851	11.828	7.876	0.69	19.022	15.916	7.312	0.301
RbSnI <sub>3</sub>	8.912	12.058	8.030	0.73	18.915	16.409	7.231	0.308
CsSnI <sub>3</sub>	8.856	12.350	8.359	0.77	19.287	17.139	7.348	0.312
FrSnI <sub>3</sub>	8.753	12.417	8.591	0.80	18.704	17.632	7.068	0.323
MASnI <sub>3</sub>	8.797	12.495	8.499	0.83	23.271	19.104	8.971	0.297
KSnBr <sub>3</sub>	8.292	11.073	7.469	0.69	20.645	19.176	7.817	0.321
RbSnBr <sub>3</sub>	8.345	11.348	7.623	0.73	20.473	19.625	7.719	0.326
CsSnBr <sub>3</sub>	8.289	11.629	7.928	0.78	20.920	20.801	7.851	0.332
FrSnBr <sub>3</sub>	8.182	11.650	8.178	0.80	24.978	22.486	9.498	0.315
MASnBr <sub>3</sub>	8.492	11.753	7.895	0.84	25.818	23.387	9.809	0.316
KSnCl <sub>3</sub>	7.899	10.574	7.172	0.69	23.939	23.016	9.022	0.327
RbSnCl <sub>3</sub>	7.950	10.856	7.333	0.73	22.353	23.020	8.352	0.338
CsSnCl <sub>3</sub>	7.837	11.119	7.701	0.78	24.519	25.448	9.153	0.339
FrSnCl <sub>3</sub>	7.824	11.131	7.860	0.81	29.611	26.096	11.294	0.311
MASnCl <sub>3</sub>	8.281	11.232	7.481	0.85	30.836	27.927	11.716	0.316

## 8. Stiffness tensor

**Table S4** | Computed components of the stiffness tensor  $C_{ij}$  (GPa) for all halide perovskites.

	$C_{11}$	$C_{22}$	$C_{33}$	$C_{44}$	$C_{55}$	$C_{66}$	$C_{12}$	$C_{13}$	$C_{23}$
KPbI <sub>3</sub>	35	27	17	5	12	8	10	15	10
RbPbI <sub>3</sub>	33	28	15	5	11	8	10	16	9
CsPbI <sub>3</sub>	31	34	17	6	11	7	9	17	9
FrPbI <sub>3</sub>	28	36	16	6	12	7	9	16	11
MAPbI <sub>3</sub>	25	41	31	6	10	5	8	16	13
KPbBr <sub>3</sub>	41	28	20	5	12	8	13	18	11
RbPbBr <sub>3</sub>	39	33	18	6	13	9	12	19	12
CsPbBr <sub>3</sub>	33	40	21	7	14	8	12	20	13
FrPbBr <sub>3</sub>	31	42	22	6	14	8	12	20	15
MAPbBr <sub>3</sub>	29	48	35	7	14	6	11	20	16
KPbCl <sub>3</sub>	48	32	23	6	13	9	15	22	13
RbPbCl <sub>3</sub>	43	37	22	6	13	9	15	22	15
CsPbCl <sub>3</sub>	35	46	24	7	16	8	15	23	17
FrPbCl <sub>3</sub>	35	48	28	7	17	8	13	25	17
MAPbCl <sub>3</sub>	34	53	40	7	13	7	14	20	20
KSnl <sub>3</sub>	35	29	17	5	13	8	10	16	9
RbSnI <sub>3</sub>	33	33	17	5	12	8	9	17	10
CsSnI <sub>3</sub>	27	36	21	6	12	7	9	16	10
FrSnI <sub>3</sub>	26	36	21	6	14	7	9	18	12
MASnI <sub>3</sub>	24	42	33	7	11	6	7	15	13
KSnBr <sub>3</sub>	41	32	20	5	14	9	13	20	12
RbSnBr <sub>3</sub>	38	38	20	6	13	9	12	20	13
CsSnBr <sub>3</sub>	32	43	23	7	15	7	12	21	14
FrSnBr <sub>3</sub>	34	46	31	7	19	7	10	23	13
MASnBr <sub>3</sub>	33	48	38	7	13	7	12	19	16
KSnCl <sub>3</sub>	48	36	26	6	15	10	16	24	15
RbSnCl <sub>3</sub>	43	43	23	7	15	9	15	25	16
CsSnCl <sub>3</sub>	35	49	31	8	17	8	14	25	18
FrSnCl <sub>3</sub>	39	52	41	8	22	7	11	27	14
MASnCl <sub>3</sub>	42	54	43	9	16	9	16	23	17

## 9. Compliance tensor

**Table S5** | Computed components of the compliance tensor  $S_{ij}$  (GPa $^{-1}$ ) for all halide perovskites.

	$S_{11}$	$S_{22}$	$S_{33}$	$S_{44}$	$S_{55}$	$S_{66}$	$S_{12}$	$S_{13}$	$S_{23}$
KPbI <sub>3</sub>	0.05	0.05	0.11	0.20	0.08	0.13	0.00	-0.04	-0.03
RbPbI <sub>3</sub>	0.06	0.04	0.15	0.20	0.09	0.13	0.00	-0.07	-0.03
CsPbI <sub>3</sub>	0.07	0.03	0.14	0.17	0.09	0.14	0.00	-0.07	-0.02
FrPbI <sub>3</sub>	0.08	0.04	0.17	0.17	0.08	0.14	0.01	-0.09	-0.03
MAPbI <sub>3</sub>	0.06	0.03	0.05	0.17	0.10	0.20	0.00	-0.03	-0.01
KPbBr <sub>3</sub>	0.04	0.05	0.09	0.20	0.08	0.13	-0.01	-0.03	-0.02
RbPbBr <sub>3</sub>	0.05	0.04	0.13	0.17	0.08	0.11	0.00	-0.06	-0.03
CsPbBr <sub>3</sub>	0.07	0.03	0.13	0.14	0.07	0.13	0.00	-0.07	-0.02
FrPbBr <sub>3</sub>	0.08	0.03	0.13	0.17	0.07	0.13	0.00	-0.07	-0.03
MAPbBr <sub>3</sub>	0.06	0.02	0.05	0.14	0.07	0.17	0.00	-0.03	-0.01
KPbCl <sub>3</sub>	0.04	0.04	0.09	0.17	0.08	0.11	0.00	-0.03	-0.02
RbPbCl <sub>3</sub>	0.05	0.04	0.11	0.17	0.08	0.11	0.00	-0.05	-0.03
CsPbCl <sub>3</sub>	0.08	0.03	0.13	0.14	0.06	0.13	0.00	-0.08	-0.02
FrPbCl <sub>3</sub>	0.08	0.03	0.11	0.14	0.06	0.13	0.00	-0.07	-0.02
MAPbCl <sub>3</sub>	0.04	0.02	0.04	0.14	0.08	0.14	0.00	-0.02	-0.01
KSnI <sub>3</sub>	0.05	0.04	0.11	0.20	0.08	0.13	0.00	-0.05	-0.02
RbSnI <sub>3</sub>	0.06	0.04	0.14	0.20	0.08	0.13	0.00	-0.06	-0.02
CsSnI <sub>3</sub>	0.07	0.03	0.09	0.17	0.08	0.14	0.00	-0.05	-0.01
FrSnI <sub>3</sub>	0.10	0.03	0.13	0.17	0.07	0.14	0.00	-0.08	-0.02
MASnI <sub>3</sub>	0.06	0.03	0.05	0.14	0.09	0.17	0.00	-0.03	-0.01
KSnBr <sub>3</sub>	0.05	0.04	0.11	0.20	0.07	0.11	0.00	-0.05	-0.02
RbSnBr <sub>3</sub>	0.06	0.03	0.12	0.17	0.08	0.11	0.00	-0.06	-0.02
CsSnBr <sub>3</sub>	0.08	0.03	0.12	0.14	0.07	0.14	0.00	-0.07	-0.02
FrSnBr <sub>3</sub>	0.06	0.02	0.07	0.14	0.05	0.14	0.00	-0.04	-0.01
MASnBr <sub>3</sub>	0.04	0.02	0.04	0.14	0.08	0.14	0.00	-0.02	-0.01
KSnCl <sub>3</sub>	0.04	0.04	0.08	0.17	0.07	0.10	0.00	-0.03	-0.02
RbSnCl <sub>3</sub>	0.06	0.03	0.14	0.14	0.07	0.11	0.00	-0.07	-0.03
CsSnCl <sub>3</sub>	0.07	0.03	0.09	0.13	0.06	0.13	0.00	-0.05	-0.02
FrSnCl <sub>3</sub>	0.05	0.02	0.05	0.13	0.05	0.14	0.00	-0.03	-0.01
MASnCl <sub>3</sub>	0.03	0.02	0.03	0.11	0.06	0.11	-0.01	-0.02	-0.01

## 10. Bulk modulus $B$

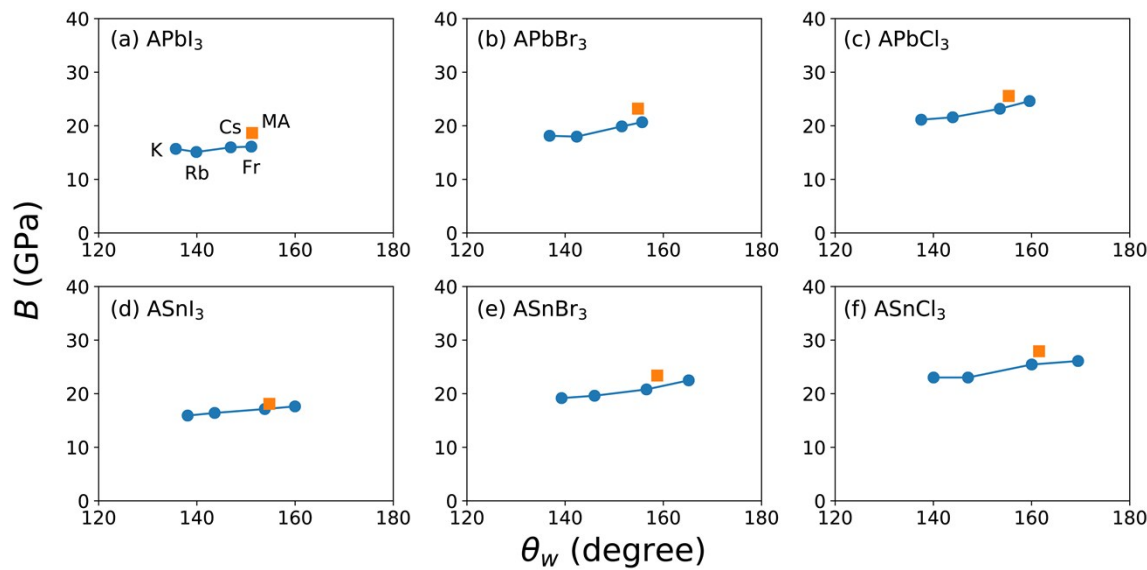


**Figure S5** | The polycrystalline bulk modulus  $B$  versus  $\theta_w$  for (a)  $\text{o-APbI}_3$ , (b)  $\text{o-APbBr}_3$ , (c)  $\text{o-APbCl}_3$ , (d)  $\text{o-ASnI}_3$ , (e)  $\text{o-ASnBr}_3$ , and (f)  $\text{o-ASnCl}_3$ . Blue and orange symbols correspond to the  $\text{o-ABX}_3$  inorganic and  $\text{o-MABX}_3$  hybrid halide perovskites respectively.

## 11. Shear modulus $G$

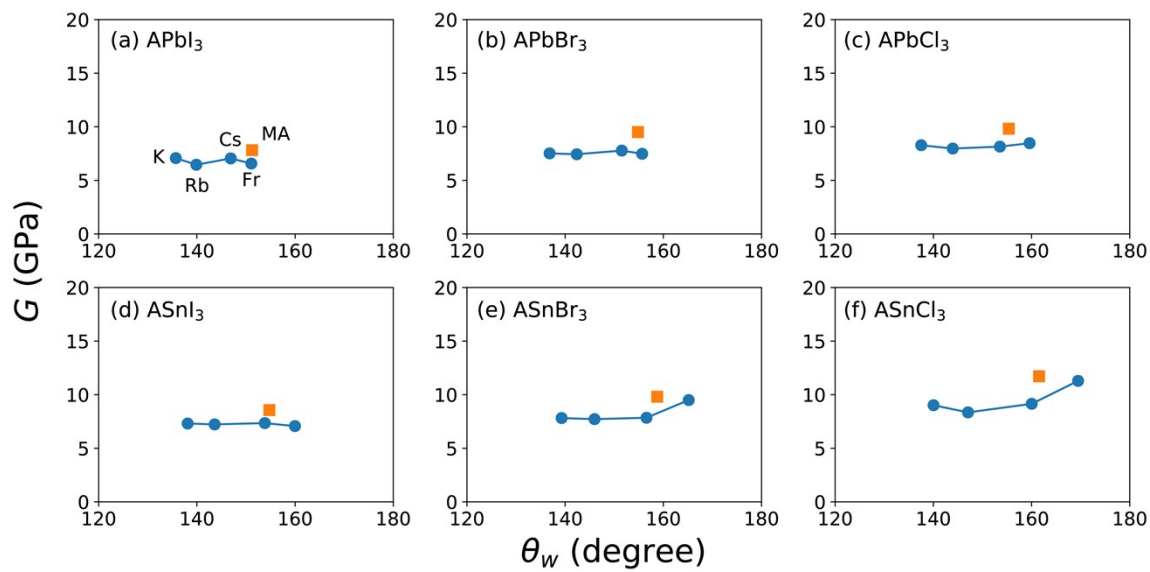


**Figure S6** | The polycrystalline shear modulus  $G$  versus  $\theta_w$  for (a)  $\text{o-APbI}_3$ , (b)  $\text{o-APbBr}_3$ , (c)  $\text{o-APbCl}_3$ , (d)  $\text{o-ASnI}_3$ , (e)  $\text{o-ASnBr}_3$ , and (f)  $\text{o-ASnCl}_3$ . Blue and orange symbols correspond to the  $\text{o-ABX}_3$  inorganic and  $\text{o-MABX}_3$  hybrid halide perovskites respectively.

**12. Orientation of the hydrogen atoms along the *b*- and *c*-axes in o-MAPbI<sub>3</sub>**

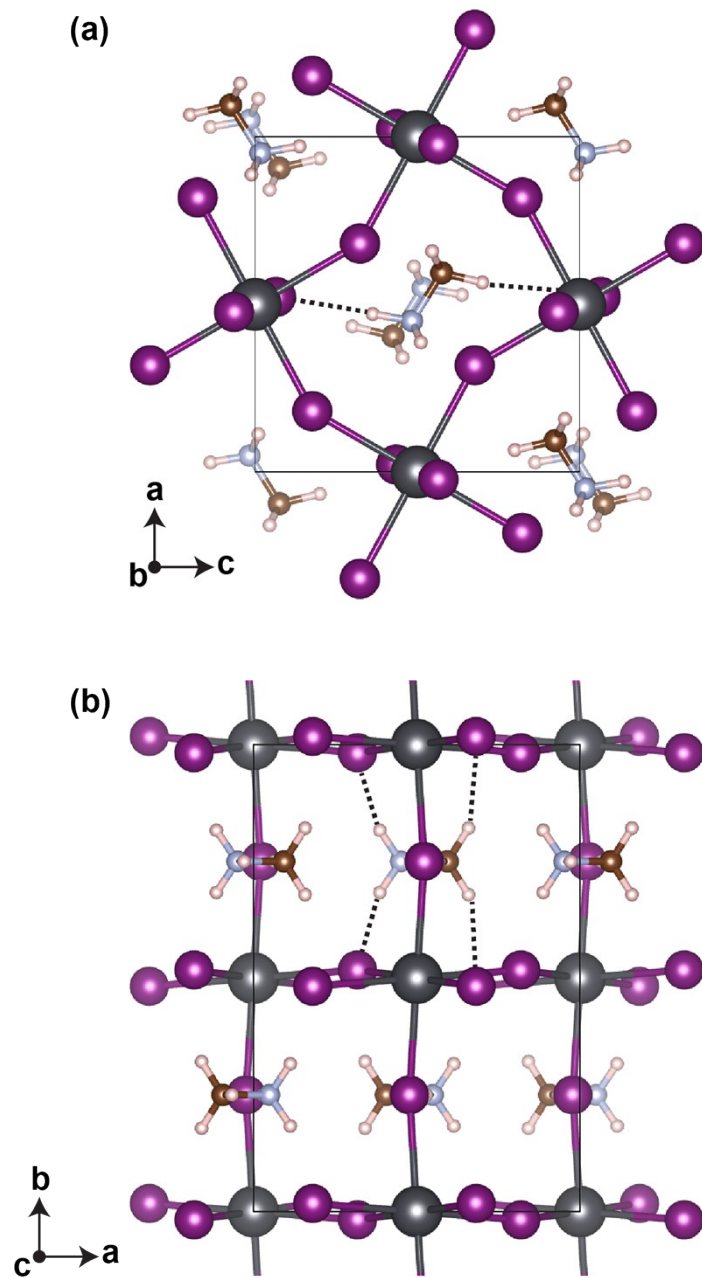


**Figure S7** | (a) *ac* plane of o-MAPbI<sub>3</sub> showing two H atoms on a MA cation oriented along the *c*-axis. (b) *ab* plane showing the other four H atoms on the MA cation oriented towards the *b*-axis. Dotted lines indicate hydrogen-bonding interactions between H and I atoms.

### 13. Deformation potentials

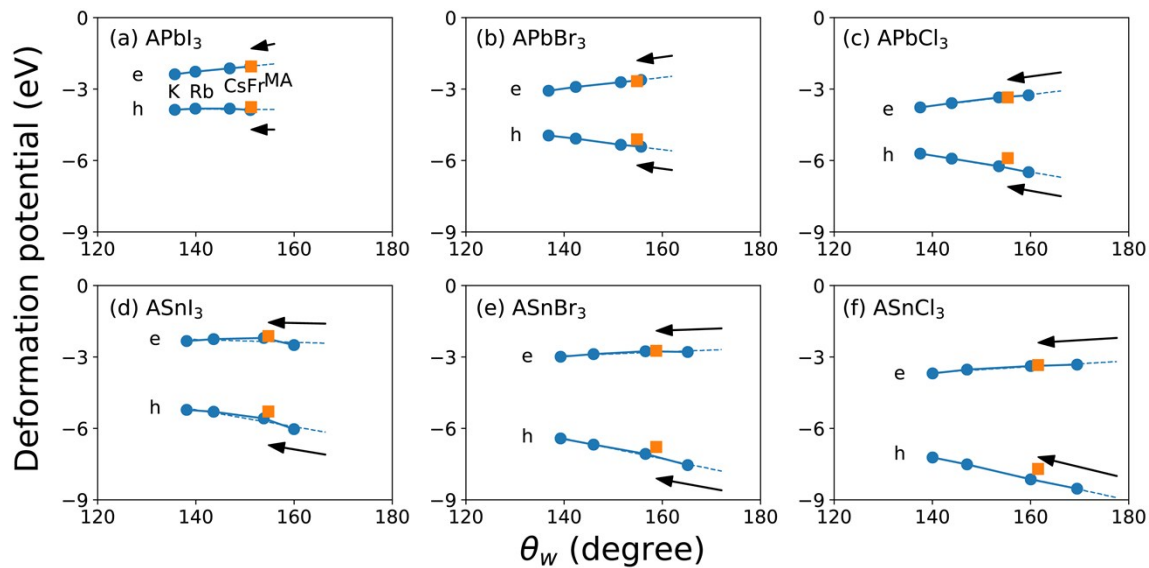


**Figure S8** | Average deformation potential along the three crystal axes versus  $\theta_w$  for (a) o-APbI<sub>3</sub>, (b) o-APbBr<sub>3</sub>, (c) o-APbCl<sub>3</sub>, (d) o-ASnI<sub>3</sub>, (e) o-ASnBr<sub>3</sub>, and (f) o-ASnCl<sub>3</sub>. Blue and orange symbols correspond to the o-ABX<sub>3</sub> inorganic and o-MABX<sub>3</sub> hybrid series respectively. Arrows represent variations of electron (e) and hole (h) deformation potentials caused by hydrogen-bonding induced octahedral tilting.

#### Notes on deformation potential calculation

We found that the deformation potential is very sensitive to the reference states chosen for the alignment of the eigenvalues during fitting. Many references were tested for band alignment including the Cl/Br/I 1s, Pb/Sn 1s and C/N/H/K/Rb/Cs/Fr 1s states but we found that the Cl/Br/I 1s core state produces the best reasonable value for linear least square fitting.

**Table S6** | Computed electron (e) and hole (h) deformation potentials  $D$  (eV) along the  $a$  [100],  $b$  [010], and  $c$  [001] axes for all halide perovskites.

	$D_h$ [100] <sub>a</sub>	$D_e$ [100] <sub>a</sub>	$D_h$ [010] <sub>b</sub>	$D_e$ [010] <sub>b</sub>	$D_h$ [001] <sub>c</sub>	$D_e$ [001] <sub>c</sub>
KPbI <sub>3</sub>	-4.16	-3.61	-3.65	-2.12	-3.80	-1.39
RbPbI <sub>3</sub>	-4.08	-3.25	-3.84	-2.08	-3.53	-1.49
CsPbI <sub>3</sub>	-4.00	-2.62	-4.11	-2.08	-3.33	-1.68
FrPbI <sub>3</sub>	-4.03	-2.30	-4.15	-2.08	-3.46	-1.77
MAPbI <sub>3</sub>	-4.11	-1.98	-3.27	-2.14	-3.90	-2.04
KPbBr <sub>3</sub>	-5.17	-4.16	-4.70	-2.87	-4.98	-2.18
RbPbBr <sub>3</sub>	-5.27	-3.81	-5.26	-2.77	-4.71	-2.15
CsPbBr <sub>3</sub>	-5.49	-3.19	-5.69	-2.68	-4.84	-2.27
FrPbBr <sub>3</sub>	-5.55	-2.89	-5.69	-2.69	-5.01	-2.29
MAPbBr <sub>3</sub>	-5.76	-2.91	-4.65	-2.69	-4.91	-2.41
KPbCl <sub>3</sub>	-5.86	-4.79	-5.58	-3.60	-5.68	-2.90
RbPbCl <sub>3</sub>	-6.08	-4.47	-6.08	-3.44	-5.61	-2.87
CsPbCl <sub>3</sub>	-6.33	-3.82	-6.60	-3.35	-5.77	-2.88
FrPbCl <sub>3</sub>	-6.40	-3.32	-6.75	-3.41	-6.31	-3.05
MAPbCl <sub>3</sub>	-6.71	-3.83	-5.48	-3.30	-5.51	-2.93
KSnI <sub>3</sub>	-5.58	-4.74	-5.09	-1.48	-5.00	-0.77
RbSnI <sub>3</sub>	-5.57	-4.03	-5.47	-1.75	-4.86	-0.97
CsSnI <sub>3</sub>	-5.72	-2.60	-5.85	-2.59	-5.18	-1.41
FrSnI <sub>3</sub>	-6.01	-2.40	-6.21	-3.09	-5.86	-2.01
MASnI <sub>3</sub>	-5.71	-1.61	-4.82	-3.18	-5.34	-1.58
KSnBr <sub>3</sub>	-6.72	-5.32	-6.25	-2.16	-6.30	-1.49
RbSnBr <sub>3</sub>	-6.90	-4.57	-6.93	-2.41	-6.22	-1.66
CsSnBr <sub>3</sub>	-7.18	-3.17	-7.39	-3.09	-6.65	-2.03
FrSnBr <sub>3</sub>	-7.36	-2.59	-7.78	-3.24	-7.48	-2.53
MASnBr <sub>3</sub>	-7.55	-2.94	-6.45	-3.24	-6.36	-2.05
KSnCl <sub>3</sub>	-7.47	-5.97	-7.06	-2.86	-7.13	-2.23
RbSnCl <sub>3</sub>	-7.70	-5.23	-7.79	-3.03	-7.05	-2.33
CsSnCl <sub>3</sub>	-8.06	-3.47	-8.44	-3.75	-7.92	-2.90
FrSnCl <sub>3</sub>	-8.31	-3.06	-8.79	-3.69	-8.51	-3.22
MASnCl <sub>3</sub>	-8.81	-4.17	-7.45	-3.47	-6.83	-2.37

## 14. Effective charge carrier masses

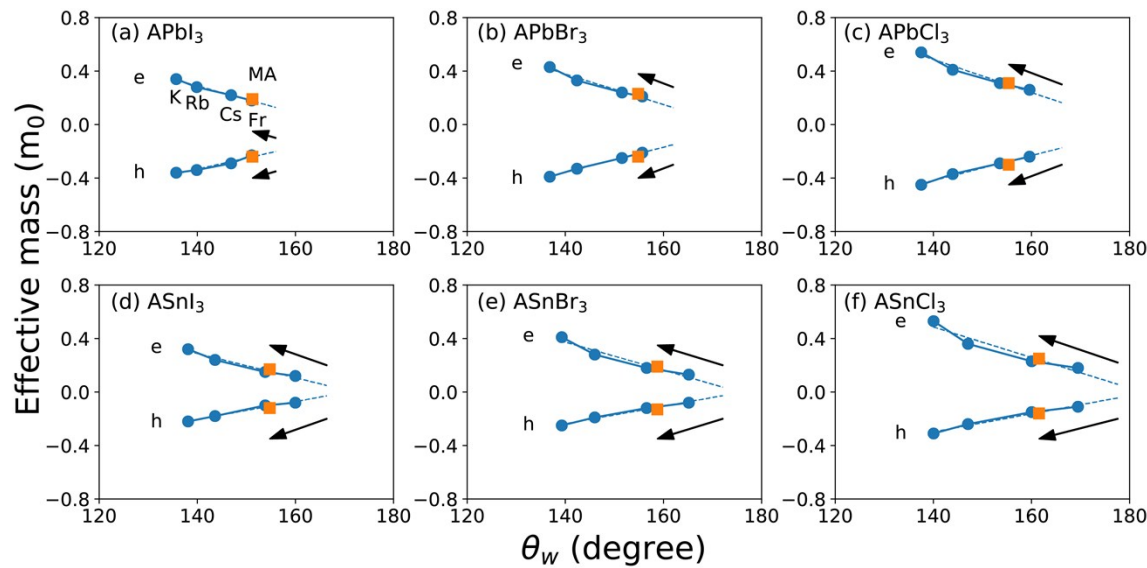


**Figure S9** | Average effective carrier mass along the three crystal axes versus  $\theta_w$  for (a)  $\text{o-APbI}_3$ , (b)  $\text{o-APbBr}_3$ , (c)  $\text{o-APbCl}_3$ , (d)  $\text{o-ASnI}_3$ , (e)  $\text{o-ASnBr}_3$ , and (f)  $\text{o-ASnCl}_3$ . Blue and orange symbols correspond to the  $\text{o-ABX}_3$  inorganic and  $\text{o-MABX}_3$  hybrid series respectively. Arrows represent increases of electron (e) and hole (h) effective masses caused by hydrogen-bonding induced octahedral tilting.

**Table S7** | Computed electron (e) and hole (h) effective carrier masses  $m^*$  (in units of rest mass  $m_0$ ) along the  $a$  [100],  $b$  [010], and  $c$  [001] axes for all halide perovskites.

	$m^*_h$ [100] <sub>a</sub>	$m^*_e$ [100] <sub>a</sub>	$m^*_h$ [010] <sub>b</sub>	$m^*_e$ [010] <sub>b</sub>	$m^*_h$ [001] <sub>c</sub>	$m^*_e$ [001] <sub>c</sub>
KPbI <sub>3</sub>	0.41	0.30	0.35	0.37	0.32	0.34
RbPbI <sub>3</sub>	0.42	0.27	0.28	0.27	0.32	0.31
CsPbI <sub>3</sub>	0.40	0.24	0.20	0.16	0.28	0.26
FrPbI <sub>3</sub>	0.30	0.20	0.17	0.14	0.23	0.21
MAPbI <sub>3</sub>	0.25	0.20	0.22	0.15	0.25	0.22
KPbBr <sub>3</sub>	0.41	0.36	0.40	0.51	0.36	0.41
RbPbBr <sub>3</sub>	0.37	0.33	0.29	0.31	0.34	0.36
CsPbBr <sub>3</sub>	0.27	0.25	0.20	0.20	0.27	0.27
FrPbBr <sub>3</sub>	0.23	0.22	0.18	0.17	0.23	0.23
MAPbBr <sub>3</sub>	0.24	0.23	0.23	0.19	0.26	0.26
KPbCl <sub>3</sub>	0.46	0.46	0.46	0.62	0.43	0.53
RbPbCl <sub>3</sub>	0.39	0.39	0.34	0.41	0.38	0.44
CsPbCl <sub>3</sub>	0.30	0.32	0.25	0.26	0.31	0.34
FrPbCl <sub>3</sub>	0.25	0.27	0.22	0.23	0.25	0.27
MAPbCl <sub>3</sub>	0.28	0.31	0.29	0.28	0.32	0.35
KSnI <sub>3</sub>	0.25	0.30	0.20	0.43	0.20	0.22
RbSnI <sub>3</sub>	0.21	0.26	0.15	0.25	0.17	0.20
CsSnI <sub>3</sub>	0.12	0.18	0.08	0.11	0.11	0.16
FrSnI <sub>3</sub>	0.09	0.14	0.06	0.08	0.08	0.13
MASnI <sub>3</sub>	0.12	0.20	0.10	0.09	0.13	0.21
KSnBr <sub>3</sub>	0.26	0.34	0.25	0.63	0.23	0.26
RbSnBr <sub>3</sub>	0.21	0.30	0.16	0.31	0.19	0.23
CsSnBr <sub>3</sub>	0.13	0.22	0.10	0.14	0.13	0.19
FrSnBr <sub>3</sub>	0.09	0.14	0.07	0.10	0.08	0.14
MASnBr <sub>3</sub>	0.13	0.22	0.11	0.15	0.14	0.21
KSnCl <sub>3</sub>	0.31	0.42	0.32	0.82	0.29	0.34
RbSnCl <sub>3</sub>	0.25	0.37	0.21	0.41	0.25	0.31
CsSnCl <sub>3</sub>	0.16	0.26	0.13	0.19	0.15	0.25
FrSnCl <sub>3</sub>	0.11	0.19	0.10	0.16	0.11	0.19
MASnCl <sub>3</sub>	0.15	0.27	0.16	0.24	0.18	0.25

## 15. Charge carrier mobility

**Table S8** | Computed electron (e) and hole (h) mobilities  $\mu$  ( $\text{cm}^2/\text{V}\cdot\text{s}$ ) at 100 K along the  $a$  [100],  $b$  [010], and  $c$  [001] axes for all halide perovskites.

	$\mu_h$ [100] <sub>a</sub>	$\mu_e$ [100] <sub>a</sub>	$\mu_h$ [010] <sub>b</sub>	$\mu_e$ [010] <sub>b</sub>	$\mu_h$ [001] <sub>c</sub>	$\mu_e$ [001] <sub>c</sub>
KPbI <sub>3</sub>	5930	17165	8733	22448	6609	42306
RbPbI <sub>3</sub>	5546	26323	14609	54387	6664	40847
CsPbI <sub>3</sub>	5981	50044	35703	242819	11641	55487
FrPbI <sub>3</sub>	11141	93714	55729	360166	16804	80425
MAPbI <sub>3</sub>	15097	114133	53960	327720	20880	105133
KPbBr <sub>3</sub>	4491	9626	4044	5896	3221	12166
RbPbBr <sub>3</sub>	5317	13553	8294	25353	3790	15839
CsPbBr <sub>3</sub>	9322	33522	22139	99755	7489	34142
FrPbBr <sub>3</sub>	12553	51667	30289	156021	10889	52270
MAPbBr <sub>3</sub>	9802	42855	27554	132713	13505	55900
KPbCl <sub>3</sub>	3072	4588	2272	2585	1865	4239
RbPbCl <sub>3</sub>	3907	7245	4758	9338	2500	6640
CsPbCl <sub>3</sub>	5643	13162	10640	37502	4316	13775
FrPbCl <sub>3</sub>	8659	26517	14712	51644	7177	25367
MAPbCl <sub>3</sub>	5747	13663	12382	37226	7178	20284
KSnl <sub>3</sub>	11285	9899	20020	34988	12309	411248
RbSnI <sub>3</sub>	16686	18641	39857	108325	19624	326311
CsSnI <sub>3</sub>	52805	92935	185905	427905	60411	321156
FrSnI <sub>3</sub>	94117	195595	334177	657575	108550	273596
MASnI <sub>3</sub>	47349	167268	180799	540424	60092	206966
KSnBr <sub>3</sub>	8308	6786	8340	6943	6441	84314
RbSnBr <sub>3</sub>	12523	11714	24518	38759	10480	91602
CsSnBr <sub>3</sub>	31990	44112	79639	196194	26678	110970
FrSnBr <sub>3</sub>	81224	216451	187772	443736	98322	212853
MASnBr <sub>3</sub>	29772	52624	91449	166398	40792	143043
KSnCl <sub>3</sub>	5062	3712	3912	2264	3532	24285
RbSnCl <sub>3</sub>	7389	6012	11127	13783	4784	25651
CsSnCl <sub>3</sub>	16700	26746	36054	70623	18021	37377
FrSnCl <sub>3</sub>	45119	84782	67936	119297	44671	79477
MASnCl <sub>3</sub>	19877	20437	30360	50788	21167	77164

**Table S9** | Computed electron (e) and hole (h) mobilities  $\mu$  ( $\text{cm}^2/\text{V}\cdot\text{s}$ ) at 300 K along the *a* [100], *b* [010], and *c* [001] axes for all halide perovskites.

	$\mu_h$ [100] <sub>a</sub>	$\mu_e$ [100] <sub>a</sub>	$\mu_h$ [010] <sub>b</sub>	$\mu_e$ [010] <sub>b</sub>	$\mu_h$ [001] <sub>c</sub>	$\mu_e$ [001] <sub>c</sub>
KPbI <sub>3</sub>	1137	3301	1689	4429	1242	7994
RbPbI <sub>3</sub>	1077	4903	2692	10464	1293	8108
CsPbI <sub>3</sub>	1157	9758	7157	44701	2271	10951
FrPbI <sub>3</sub>	2181	17536	10607	74258	3116	15131
MAPbI <sub>3</sub>	2986	21668	10747	64657	3825	21029
KPbBr <sub>3</sub>	862	1821	762	1127	637	2412
RbPbBr <sub>3</sub>	1015	2708	1625	4721	726	2992
CsPbBr <sub>3</sub>	1737	6255	4187	19861	1504	6528
FrPbBr <sub>3</sub>	2309	9528	5645	29195	2064	9602
MAPbBr <sub>3</sub>	1925	8076	5237	24025	2684	10643
KPbCl <sub>3</sub>	576	871	445	501	365	834
RbPbCl <sub>3</sub>	748	1372	892	1769	468	1313
CsPbCl <sub>3</sub>	1061	2587	2140	6995	838	2705
FrPbCl <sub>3</sub>	1638	5137	2830	9763	1409	4801
MAPbCl <sub>3</sub>	1082	2695	2388	7477	1345	3790
KSnl <sub>3</sub>	2278	1973	3677	6664	2343	78177
RbSnI <sub>3</sub>	3264	3657	8251	20108	3592	66035
CsSnI <sub>3</sub>	9313	16868	33249	88977	11546	66044
FrSnI <sub>3</sub>	20031	40155	61048	134985	19829	53838
MASnI <sub>3</sub>	8231	33449	38204	95096	12068	39757
KSnBr <sub>3</sub>	1541	1282	1607	1337	1213	16006
RbSnBr <sub>3</sub>	2446	2280	4497	7331	1975	17409
CsSnBr <sub>3</sub>	6001	8585	15720	36005	5589	21583
FrSnBr <sub>3</sub>	17531	39083	35911	75835	17174	41338
MASnBr <sub>3</sub>	6306	10700	15776	33699	8352	27283
KSnCl <sub>3</sub>	951	726	780	434	667	4530
RbSnCl <sub>3</sub>	1412	1146	2102	2587	963	4972
CsSnCl <sub>3</sub>	3460	5028	6956	12886	3363	7539
FrSnCl <sub>3</sub>	8238	17285	12194	21463	8502	15883
MASnCl <sub>3</sub>	3703	3875	5853	9584	4125	14372

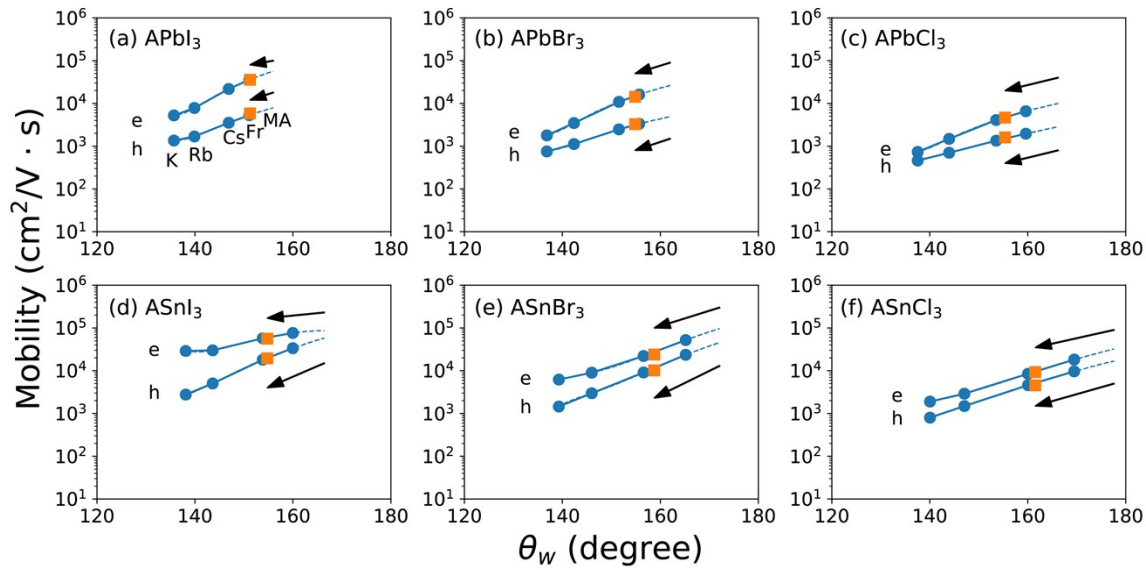


**Figure S10** | Average electron (e) and hole (h) mobilities along the three crystal axes versus  $\theta_w$  for (a)  $\text{o-APbI}_3$ , (b)  $\text{o-APbBr}_3$ , (c)  $\text{o-APbCl}_3$ , (d)  $\text{o-ASnI}_3$ , (e)  $\text{o-ASnBr}_3$ , and (f)  $\text{o-ASnCl}_3$ . Blue and orange symbols correspond to  $\text{o-ABX}_3$  inorganic and  $\text{o-MABX}_3$  hybrid halide perovskites, respectively. Arrows indicate the reduction in the e and h mobilities of  $\text{o-MABX}_3$  with respect to what they would have been for hypothetical  $\text{o-ABX}_3$  perovskites having the same size A-site cation. The arrows follow the extrapolated trend lines. The values are calculated at 300 K.

## References

- 1 J. P. Perdew, A. Ruzsinszky, G. I. Csonka, O. A. Vydrov, G. E. Scuseria, L. A. Constantin, X. Zhou and K. Burke, *Phys. Rev. Lett.*, 2008, **100**, 136406.
- 2 J. Klimeš, D. R. Bowler and A. Michaelides, *J. Phys. Condens. Matter*, 2010, **22**, 022201.
- 3 J. Klimeš, D. R. Bowler and A. Michaelides, *Phys. Rev. B*, 2011, **83**, 195131.
- 4 K. Lee, É. D. Murray, L. Kong, B. I. Lundqvist and D. C. Langreth, *Phys. Rev. B*, 2010, **82**, 081101.
- 5 A. Tkatchenko and M. Scheffler, *Phys. Rev. Lett.*, 2009, **102**, 6–9.
- 6 J. Sun, A. Ruzsinszky and J. P. Perdew, *Phys. Rev. Lett.*, 2015, **115**, 036402.
- 7 M. T. Weller, O. J. Weber, P. F. Henry, A. M. Di Pumbo and T. C. Hansen, *Chem. Commun.*, 2015, **51**, 4180–4183.
- 8 R. D. Shannon, *Acta Cryst.*, 1976, **A32**, 751–767.